https://doi.org/10.1016/j.jsv.2021.116102

Complete Sub-Wavelength Flexural Wave Band Gaps in Plates with Periodic Acoustic Black Holes

Liling Tang,[a b*] Li Cheng,[c] Kean Chen[a b]

[a] *School of Marine Science and Technology, Northwestern Polytechnical University, Xi'an, China*

[b] *Key Laboratory of Ocean Acoustics and Sensing, Northwestern Polytechnical University, Ministry of Industry and Information Technology, Xi'an, China*

[c] *Department of Mechanical Engineering, The Hong Kong Polytechnic University, Hung Hom, Kowloon, Hong Kong, China*

[*]Corresponding author: liling.tang@nwpu.edu.cn

Abstract

Acoustic Black Hole (ABH) effect shows promise for vibration control, but mainly limited to a relatively high frequency range. Though achievable in 1D periodic ABH structures, complete sub-wavelength band gaps (BGs) have not yet been realized in 2D configuration. Capitalizing on the unique wave propagation characteristics of the ABH, we propose a new type of plates containing periodically arranged double-layer ABH cells which offer complete and omnidirectional BGs. The phenomena originate from the combined effects of the ABH-specific local resonances and Bragg scattering, which are made possible through a dual process: a proper channeling of the wave propagation path and an impaired coupling between the ABH-induced local resonances and the global vibration of the unit cells. The former is warranted by a proper structural tailoring of the unit cells and the latter by the dynamics of the double-layer ABH design. It is shown that the BGs can be tuned through adjusting ABH parameters. Meanwhile, attaching the centers of the double ABH branches with a connecting cylinder can further broaden and lower the frequencies of the BGs as a result of the enhanced Bragg scattering. It is also demonstrated numerically and experimentally that remarkable vibration attenuation and energy insulation can be achieved in a plate with only a small number of ABH

cells, thus pointing at the possibility of achieving sub-wavelength vibration control in structures with reasonable dimensions.

Keywords: *Periodic plates; complete sub-wavelength band gaps; acoustic black hole; vibration attenuation; flexural waves.*

1. Introduction

The Acoustic Black Hole (ABH) effect features unique wave propagation characteristics inside a structure whose thickness is tailored according to a power-law relationship. With the decreasing structural thickness, the local phase/group velocity of flexural waves gradually reduces, ideally to zero with no wave reflection when the thickness diminishes [1, 2]. The resultant energy focusing phenomenon within the ABH region offers new possibilities for applications such as vibration control [3-6], sound radiation reduction [7-10] and energy harvesting [11-13].

Single ABH element/structure has been widely investigated with demonstrated effectiveness for vibration attenuation [14-20]. However, systematic broadband ABH effects can only be achieved above a certain frequency, referred to as cut-on frequency in the literature, when the incoming wavelength is comparable to or smaller than the characteristic dimension of the ABH element [7, 21]. Therefore, for the lower frequency range, the dimension of an ABH element would become prohibitively large, which seriously hampers practical applications. Therefore, realizing sub-wavelength control is a bottle-necking problem of paramount importance, considering the imperious demands in extending ABH effect to a lower frequency region in structures of reasonable dimensions.

Structures embedded with multiple or periodic ABH elements may provide a feasible means to solve this dilemma. For 1D beam structures with periodic ABH cells, we have firstly demonstrated that, through a proper combination of local resonances and Bragg scattering, broad band gaps (BGs) can be achieved over a wide frequency range, including the low frequency one [22, 23]. Subsequently, various ABH-based designs of periodic beams were exploited, exemplified by V-folded beams [24],

graded ABHs [25] and composite ABHs [26] *etc*. The above existing efforts, however, were limited to 1D configuration, in which wave propagation takes place in a relatively simple and easy-to-control manner. For 2D structures such as a plate, periodic ABHs have been explored to realize exotic wave propagation phenomena such as bi-refraction [27] or to conceive specific acoustic devices such as acoustic lens [28] and topological elastic waveguides [29]. However, different from 1D case, wave propagation mode/paths in 2D ABH plates are much more complex. As a result, only directional BGs, which prohibit wave propagation along the direction perpendicular to a width-through ABH tunnel, were achieved in our previous work [30, 31]. Therefore, complete BGs in periodic 2D ABH plates have not been materialized yet up to now.

Motivated by this, we propose here the design of a new type of compound plates containing periodically arranged double-layer ABH cells. By capitalizing on the unique wave propagation characteristics of the ABH, the proposed structure is shown to exhibit complete and omnidirectional BGs, conducive to applications such as vibration attenuation and energy insulation of flexural waves. Apart from the demonstration of the superior BG properties of the plates, the underlying mechanism behind the BG formation is also revealed, thus showing another novelty of the work.

The paper is organized as follows. The underlying design philosophy of the proposed 2D ABH plates and their wave propagation characteristics are first analyzed. Complete sub-wavelength BGs and the underlying mechanism are then demonstrated and analyzed through numerical simulations. Ways to increase the BG performance are then exploited, including the tuning of the ABH parameters and the use of additional structural elements to broaden the BGs. Then, experiments are conducted to validate the numerically predicted phenomena. Finally, conclusions are drawn.

2. Periodic plates embedded with 2D ABHs

2.1 Wave propagation in 2D ABH plates

Figure 1(a) shows a uniform plate element carved inside with a 2D ABH indentation whose thickness, *h(r)*, is tailored according to $h(r)=\varepsilon r^m$ with *m* being the taper power index, normally larger than 2 [3]. As shown in Fig. 1(a), when flexural waves travel from the uniform part to the ABH indentation along a vector $\boldsymbol{k}$ direction, the ray trajectory is governed by Snell law [27]:

$$\frac{dr}{d\theta} = r\frac{1}{\tan\alpha}, \tag{1}$$

$$\frac{d\alpha}{d\theta} = -1-\frac{r}{n}\frac{dn}{dr}, \tag{2}$$

$$nr\sin\alpha = \text{const}, \tag{3}$$

where *r* and θ are the coordinates in a polar system with origin at the ABH center, α is the angle between $\boldsymbol{k}$ and $\boldsymbol{r}$, and $n(r)=\sqrt{h/h(r)}$ is the local refraction index with *h* and *h*(r) being the local thickness of the uniform part of the plate and that of the ABH indentation, respectively.

Typical wave propagation pattern is first qualitatively illustrated to show the underlying design philosophy. More quantitative and detailed analysis can be found in [32]. Considering an incident plane wave for instance, the wave propagation trajectory in an ideal ABH plate is sketched in Fig. 1(b). On one hand, the trajectory of the wave traveling through the ABH would be curved inside towards the ABH center, before finally being trapped at the center of the ABH indentation in the ideal zero thickness case, as shown by the red solid lines in Fig. 1(b). This process would promote a high energy concentration and rich local dynamics inside the ABH region. On the other hand, the other portion of the waves beyond the ABH region would directly pass through the uniform part of the structure as denoted by the green solid lines, jeopardizing the possible formation of BGs. Therefore, this direct wave transmission path needs to be cut through proper structural design while preserving the locally resonant effects of the ABH cells to achieve complete BGs, similar to beam structures [22, 23]. One intuitive way is to enlarge the radius of the ABH indentation so that its periphery intersects with the boundaries of the uniform plate

element, as shown in Fig. 1(c). Admittedly, in practice, a residual thickness inevitably exists at the ABH center which results in non-zero wave velocity. Nevertheless, as sketched in Fig. 1(d), the incident waves would still be concentrated and focused around the ABH center and then continue to propagate until part of the energy is reflected by the ABH boundaries and re-injected back into the indentation.

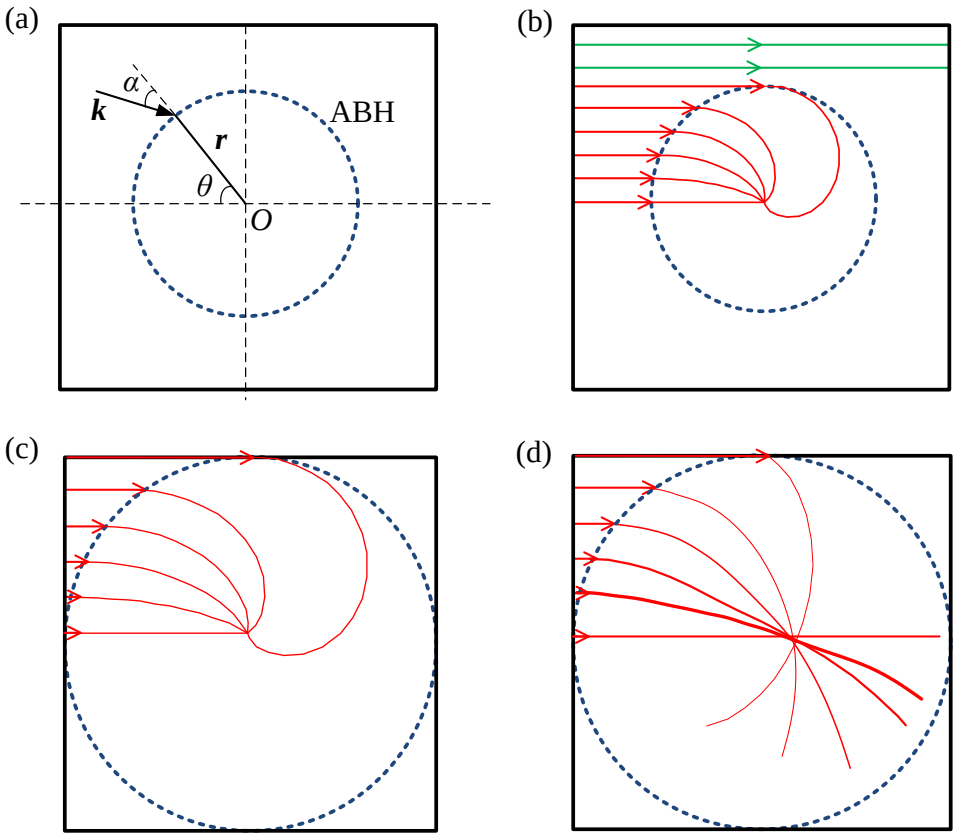

Fig. 1 Sketch illustrating typical wave propagation in a plate embedded with a 2D ABH indentation: (a) reference system used for ray trajectory analysis; (b) uniform plate carved inside with an ideal 2D ABH indentation; (c) ideal ABH indentation with its periphery intersecting with the boundary of the plate; (d) non-ideal ABH indentation with its periphery intersecting with the boundary of the plate.

2.2 Design of periodic plates with 2D ABHs

Based on the above analyses, we propose a plate design which ensures an effective confinement of the incoming waves to the ABH indentation area, while maintaining a reasonably good structural integrity when forming a periodic lattice. It

is expected that, as long as the outer periphery of the ABH indentation and the boundary of the uniform plate element intersect with each other, all incoming waves would be forced to enter the ABH indentation area. The confined waves would eventually produce the locally resonant and scattering effects, as to be demonstrated later on. This will ultimately produce BGs when these unit cells are periodically arranged to form a lattice.

In light of these considerations, we propose a new type of compound plates, comprising double-layer periodic unit cells as shown in Fig. 2. Each unit cell is a uniform plate element excavated inside with a symmetrical circular cone tapered according to a standard ABH profile, as depicted by the blue solid in Fig. 2(a). Fig. 2(b) shows the zoomed-in cross-sectional detail of the unit cell, as encircled by a red dashed line in Fig. 2(a). The unit cell has a lattice constant a and a thickness h. The thickness of the ABH portion follows $h(x) = \varepsilon x^m + h_0$ with m and h_0 being the taper power index and the residual truncation thickness, respectively. To ensure the intersecting conditions as well as the structural integrity of the element, the radial length of ABH l_{ABH} and the lattice constant a should satisfy $\sqrt{2}l_{\mathrm{ABH}} < a < 2l_{\mathrm{ABH}}$. Here, $a=\sqrt{2}l_{\mathrm{ABH}}$ and $2l_{\mathrm{ABH}}$ correspond to the two extremum conditions when the ABH periphery is completely excircled and encircled by the unit cell, respectively. After excavation of the ABH circular cone, the unit cell is formed as shown in Fig. 2(c). Such a design guarantees the structural integrity in terms of both lattice surface and a reasonable overall structural stiffness and strength, different from the conventional ABH design in which ABH indentation is usually carved inside the plate.

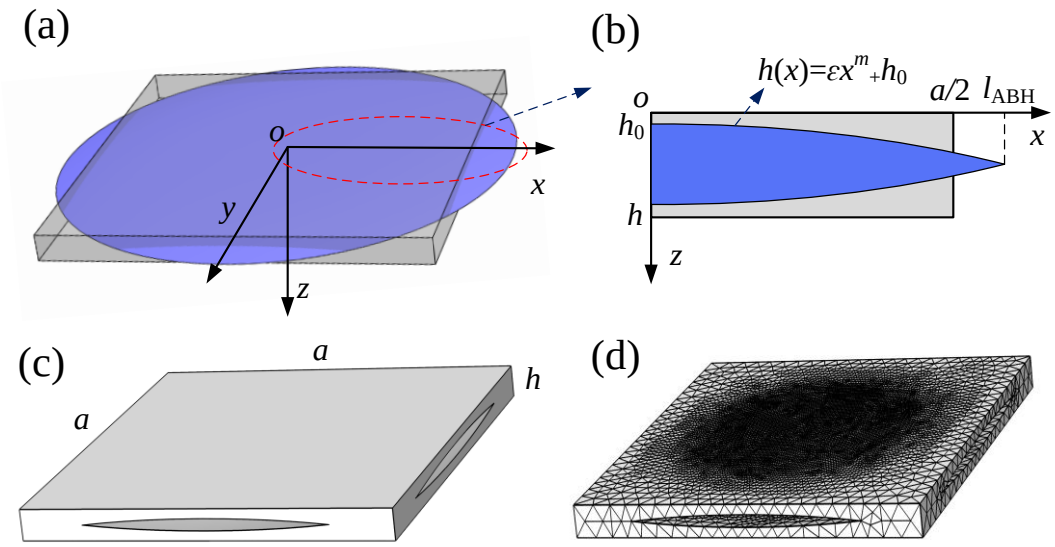

Fig. 2 (a) Unit cell of a periodic plate with a uniform plate element excavated inside by a symmetrical ABH circular cone as denoted by the blue solid; (b) Local cross section of the unit cell as circled by the red dash line in Fig. 2(a), where the thickness of ABH profile follows $h(x) = \varepsilon x^m + h_0$; (c) sketch of the unit cell; (d) FE mesh of the unit cell.

3. Numerical results and analyses

Finite element analysis using COMSOL Multiphysics 5.2 is carried out. For an infinite plate, Floquet-Bloch perioidc boudary conditions are imposed at the edges of the unit cell in both x and y directions. A parametric sweep of reduced wavevector $k\pi/a$ is applied over the first irreducible Brilliouin zone. The mesh is physics-controlled with tetrahedral elements in finer element size to ensure the convergence of the computation, shown in Fig. 2(d). The material is alumimum with a mass density of 2700 kg/m^3, Young's modulus of 70 Gpa and Poisson ratio of 0.3. The initial structural demensions are: h=7.08 mm, h_0=0.3mm, m=3, l_{ABH} =60 mm, and a=100 mm. The structural dimension is subject to change in the following parametric analyses whenever needed.

3.1 Formation of complete sub-wavelength band gaps

The calculated band structures are presented in Fig. 3, in which blue circles denote flexural waves, red circles S0 waves and green circles SH0 waves. Detailed analyses and discussions on S0 and SH0 waves, which are beyond the interest scope of this work, can be found in Ref. [30]. We shall only focus on flexural waves, which are excited by out-of-plane excitations and more relevant to vibration and sound radiation problems in flexible structures. To better quantify the phenomena, a normalized frequency $f_R = fa/c$ is defined and included as the right-hand-side vertical coordinate to eliminate the actual size effect, with c being the flexural wave velocity in the uniform part of the plate. It can be seen that, several broad directional flexural wave BGs along Γ-X appear, as marked inside the grey areas. More importantly, two complete flexural wave BGs (marked by pink areas) appear in two frequency ranges from 904 Hz to 1262 Hz and from 1364 Hz to 1467 Hz, respectively. The corresponding normalized frequencies are around 0.15, one order of magnitude lower than the characteristic frequency c/a of the unit cell. Namely, the periodic plates exhibit complete, omnidirectional and sub-wavelength flexural wave BGs at a reduced frequency range.

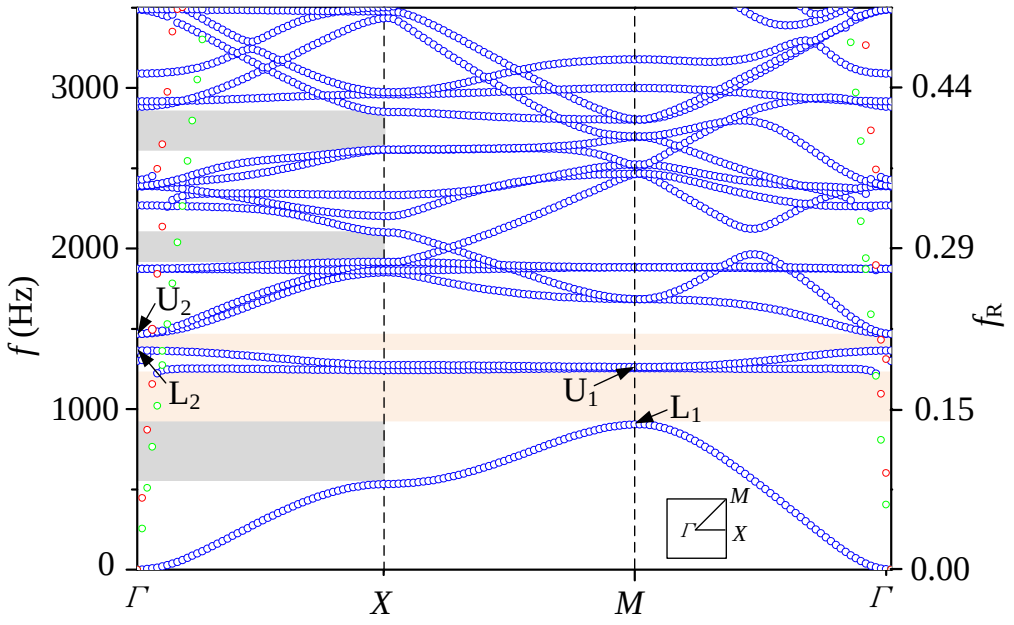

Fig. 3 Band structures with blue, red and green circles denoting flexural, S0 and SH0 waves, respectively.

3.2 Underlying formation mechanism of the BGs

To understand the underlying mechanism behind the formation of the observed BGs, eigenmodes at the edge points as labeled in Fig. 3 are shown in Fig. 4 in terms of normalized vibration displacement. For the first BG, the eigenmode at the upper edge U_1 shows accentuated vibration within the central area of the ABH indentations with out of phase and negligible vibration on the uniform part of the plate element, thus exhibiting strongly local resonances. The nearly flat dispersion curves also confirm the fact that waves with zero group velocity would be trapped inside the ABH which can hardly propagate forward. The eigenmode at the lower edge L_1, on the contrary, involves global vibration of the element with strong anti-symmetrical motion at its four corners, typical of the Bragg scattering effect. Indeed, from the wave propagation perspective, for the practical ABH taper with a residual thickness, waves would be concentrated around the center of ABH and propagate forward before being reflected back by the ABH periphery and the unit cell. This process repeats itself and develops into the Bragg scattering whenever waves hit the ABH boundary. Therefore, the first BG can be attributed to the combined effects of local resonances and Bragg scattering. Similarly, the eigenmode L_2 at the lower edge of the second BG is also highly localized within the ABH with in-phase vibration. The vibration in the upper eigenmode U_2 is partly localized around the ABH center but with non-negligible structural deformation on the uniform part. Therefore, the second BG also results from the coupling between the local resonance and Bragg scattering. This dual process backs up the formation of the two complete sub-wavelength BGs with relatively broad bandwidth, which are far below the characteristic frequency c/a.

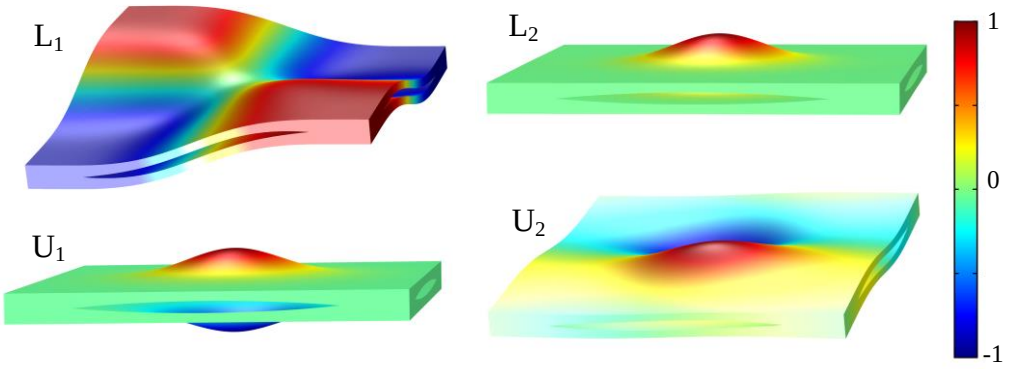

Fig. 4 Eigenmodes at edge points of the complete band gaps with normalized displacement.

As discussed in Sect. 2.1, to ensure that all incoming waves enter the ABH indentation to produce effective local resonances and the resultant BGs, the periphery of the ABH taper and the boundary of the uniform plate element should intersect with each other under $\sqrt{2}l_{\mathrm{ABH}} < a < 2l_{\mathrm{ABH}}$. To demonstrate the necessity of this condition, the effect of the normalized a/l_{ABH} on band structures is shown in Fig. 5. As expected, when a/l_{ABH} =2, corresponding to the case when the ABH cell is encircled within the uniform plate element, no complete BGs can be obtained, as shown in Fig. 5 (a), since the lowest dispersion curve corresponding to the global mode intersects with the flat dispersion curves induced by the ABH local resonances. Namely, although most waves pass through the ABH taper and generate the local resonance, part of waves, at the same time, still escape from the small margin in the uniform part. When further reducing a/l_{ABH}, the boundary of the ABH taper and that of the uniform plate start to intersect with each other, BGs (marked by pink areas) start to appear. Specifically, reducing a/l_{ABH} shows little effect on the dispersion curves corresponding to the local resonance since the local resonant modes are mainly dominated by the strong vibration around the center of the ABH indentation. However, the dispersion curve corresponding to the global deformation would be lower because of the reduced global stiffness. As a result, complete BGs can be achieved at even lower frequencies.

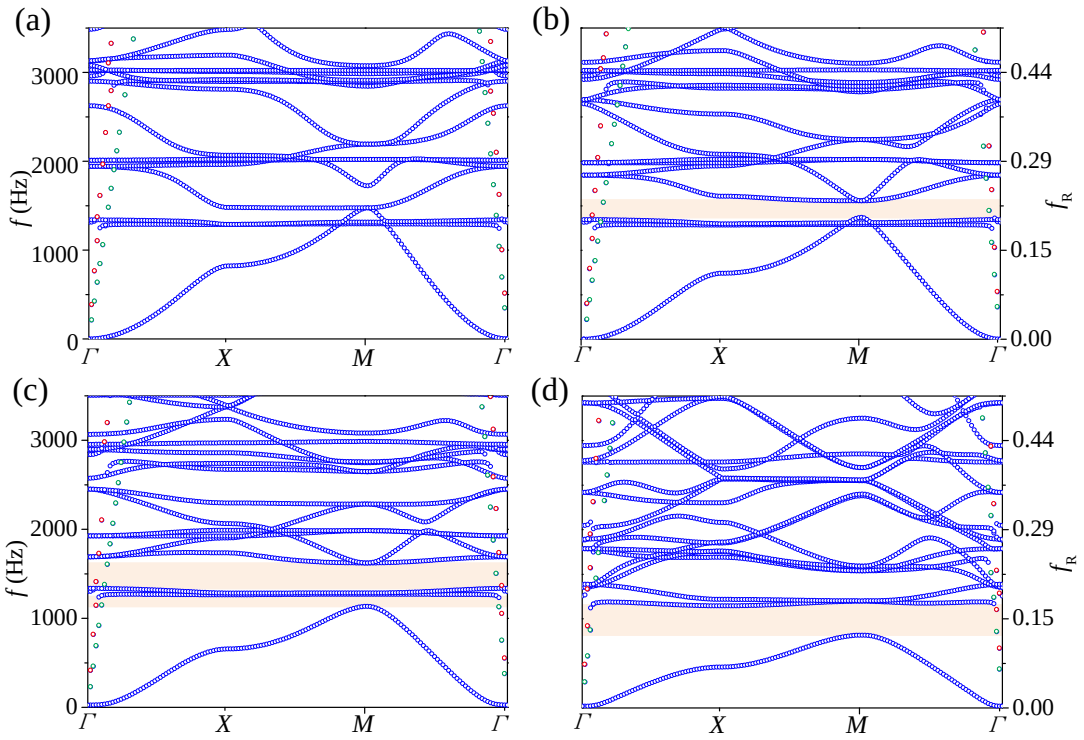

Fig. 5 Effects of normalized a/l_{ABH} on band structures with different values of lattice constant a: (a) 2; (b) 1.92; (c) 1.83; (d) 1.5.

As a comparison, Fig. 6 shows the unit cell of a conventional single-layer plate element with the same ABH geometrical parameters and the corresponding band structures. Interesting enough is the observation that complete BGs cannot be achieved even under the condition $\sqrt{2}l_{ABH} < a < 2l_{ABH}$. As can be seen, different from the band structures of the compound plates in Fig. 3, flat dispersion curves representing local resonance can only be observed along Γ to M, rather than over the whole first irreducible Brillouin zone. Some representative eigenmodes are also given in Fig. 6. It can be seen that, although locally resonant modes, exemplified by C_1, still exist, with almost the same frequency as the one shown in Fig. 3 due to the use of the same set of ABH parameters, these locally resonant vibrations are closely coupled to the global vibration of the unit cell in the lower sub-wavelength frequency range as encircled by the red dashed line, typically denoted by C_2 and C_3. As a result, the closeness of their vibration frequencies between the local resonance and the global vibration jeopardizes the formation of the BGs. Actually, for the single ABH plate

element, the ABH indentation, as part of the entire unit cell, strongly affects the overall structural stiffness of the element and therefore results in a strong coupling between the local resonance and the global vibration of the element. However, owing to the compound double-layer ABH configuration, the overall structural stiffness of the element is significantly increased as compared with its single layer counterpart. Consequently, global vibration of the element occurs at a higher frequency, further separated away from that of the local resonances. This analysis suggests that, achieving complete sub-wavelength BGs in the proposed structures relies on two main factors. The first one is to produce reduced coupling between the ABH-induced local resonances and the global vibration of the element, which is materialized by the proposed compound double-layer design. The other one is to channel all waves to propagate into the ABH indentation, which is realized by reducing the lattice constant or enlarging the ABH indentation so that its outer boundary intersects with that of the uniform plate element before forming the periodic lattice.

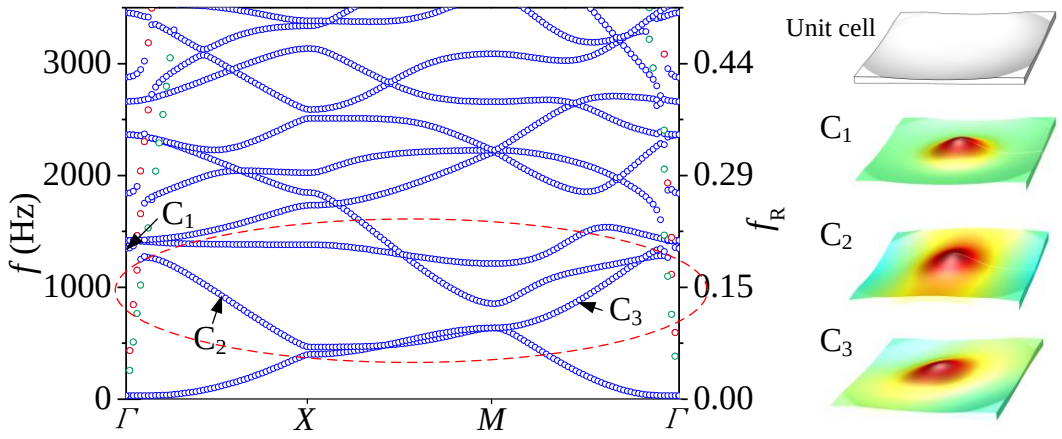

Fig. 6 Band structures of a conventional single-layer plate lattice with the same geometrical ABH parameters.

3.3 Vibration insulation in a finite plate

The vibration attenuation ability of the proposed structure is assessed using a finite freely-supported plate containing 6×4 cells. A transverse harmonic point force excitation is applied at one corner of the plate while the receiver is at the opposite

diagonal corner. A transmissibility is defined as $T = 20\log_{10}(w_{out} / w_{in})$ with w_{out} and w_{in} being the displacement amplitudes at the receiver and excitation points respectively. Results are shown in Fig.7, in which two BGs (marked by pink areas) obtained in the corresponding infinite plate are also given as reference. As can be seen, the vibration amplitude is significantly reduced within two frequency bands by as much as 80 dB across the two points with only a few ABH cells, which demonstrates the ability of the proposed plate for vibration insulation. The attenuation bands with weak transmission correspond well to the two BGs calculated using infinite plate above. The vibration displacement distributions at two typical frequencies, one inside and the other outside the attenuation band, are also provided in the figure. For 1230 Hz which is inside the first attenuation band, the vibration is basically confined to the center close to the first ABH cell and quickly attenuated in the following ones. After a few rows along the diagonal direction, vibration literally disappears on the remaining portion of the plate. This also partly confirms that this BG is attributed to the coupled effect of local resonances and Bragg scattering as discussed above. By contrast, at 2330 Hz which is outside the attenuation bands, vibration spreads over the entire plate with no noticeable attenuation along the excitation-receiver path.

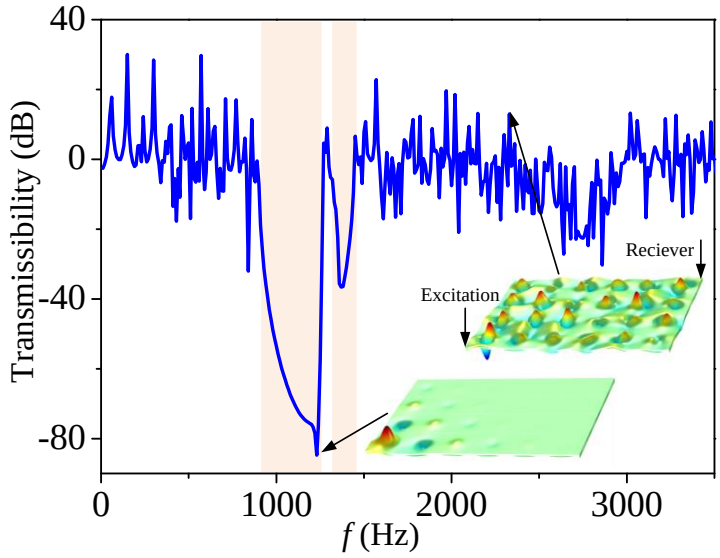

Fig. 7 Transmissibility of a finite plate with 6×4 cells. Vibration displacement field is displayed for 1230 Hz and 2330 Hz, which are inside and outside attenuation band,

respectively.

4. Methods to broaden the sub-wavelength band gaps

4.1 Tuning ABH parameters

Since the formation of the BGs is closely related to the ABH phenomena, effects of tuning ABH geometrical parameters, *i.e.* truncation thickness h_0 and taper power index m, are analyzed to seek possible ways for broadening the BGs. Variations of BGs with respect to h_0 and m are shown in Fig. 8, in which BGs are marked by blue areas whose upper and lower boundaries denote their corresponding edge frequencies. As shown in Fig. 8 (a), reducing h_0 lowers both the upper and lower boundaries of the first BG, alongside the creation of more BGs. This is understandable considering the positive effect of a smaller h_0 on reducing the local resonance frequencies. Predictably, should an ideal ABH taper with zero thickness be possible, BGs would have been achieved over the entire frequency range, which is obviously an idealized and unrealistic scenario. Similarly, increasing m would have the same effects in terms of enhancing ABH effects and the induced local resonances. As a result, lower and wider BGs can be obtained as shown in Fig. 8 (b), as long as m is not excessively large to violate the smoothness condition [33]. Therefore, we can tune the ABH geometrical parameters h_0 and m, as well as the lattice constant a, to obtain desirable sub-wavelength BGs in specific frequency ranges.

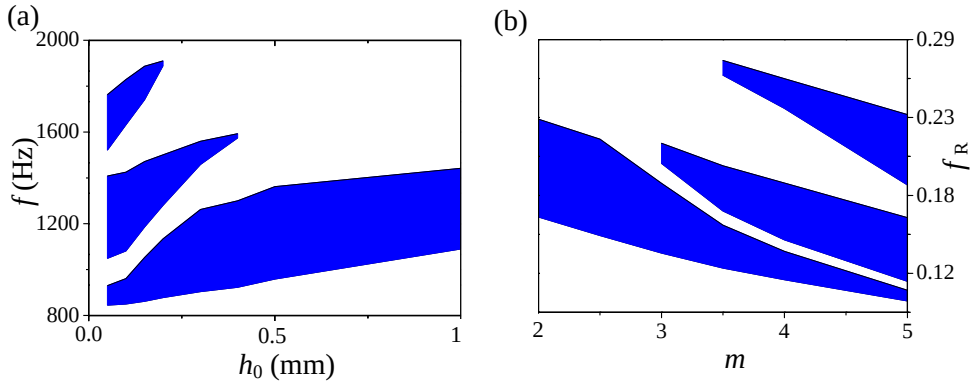

Fig. 8 Effect of (a) h_0 and (b) m on BGs as marked by blue areas. The upper and lower boundaries denote corresponding edge frequencies of the BGs.

4.2 Strengthening Bragg scattering through adding a connecting cylinder

The margin for increasing the bandwidth of BGs through the tuning of ABH geometrical parameters is, to some extent, not very large and limited by manufacturing capability and practical constraint. As an alternative, we propose adding a small cylinder with a radius r at the ABH center to connect the two ABH branches, as shown in Fig. 9. The unit cell is still a uniform plate excavated inside with a symmetrical tapered ABH profile, as depicted by the blue area in Fig. 9 (a). In so doing, the ABH area becomes a ring. As shown by a cross-sectional view in Fig. 9 (b), the thickness variation of each ABH branch follows $h(x)=\varepsilon(x-r)^m+h_0$. With all other geometrical parameters remaining the same as before, the actual length of ABH taper becomes l_{ABH}-r. The final unit cell is sketched in Fig. 9 (c). The additional connecting cylinder, through attaching the two ABH branches at the center would avoid the use of extremely thin truncation thickness within the indented area, thus increasing the both the local and overall stiffness of the element. More importantly, its use would create a large impedance mismatch/discontinuity with the surrounding thin ABH indentation, so as to generate more pronounced Bragg scattering to broaden the resultant BGs.

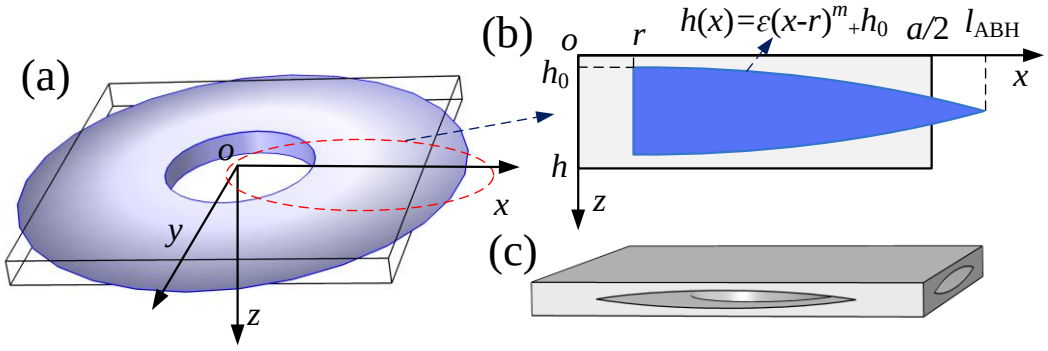

Fig. 9 Unit cell of periodic 2D ABH plates with additional connecting cylinder.

With this disposition, Fig. 10 shows the corresponding band structures with a connecting cylinder with r=20 mm while other parameters being kept the same as used in Fig. 3. Compared with Fig. 3, a broader complete sub-wavelength BG marked by pink area is achieved from 751 Hz to 1664 Hz, corresponding to the normalized

frequency range from 0.11 to 0.24. The obtained bandwidth basically doubles the one obtained without the connecting cylinder (Fig. 3). Meanwhile, the lower frequency bound of the BG is also shifted from 904 Hz to 751 Hz, which further maximizes the low frequency benefit. The eigenmodes at some critical edge points are also presented in Fig. 10. The eigenmode L_{x1} at the lower edge of the first directional BG along Γ-X is highly localized around the ABH center. In this case, the connecting cylinder acts as a lumped mass, vibrating with the ABH indentation. Therefore, the local resonance frequency is reduced compared with that without the cylinder, shown in Fig. 3. For L_1 and U_1, more global vibration is observed, favorable to the creation of Bragg scattering effect. This is partly attributed to the fact that waves converging towards the ABH center are reflected by the connecting cylinder. The combination of the local resonances induced by ABH indentation and Bragg scattering induced by the connecting cylinder collectively produces a broad sub-wavelength BG. It can be surmised that, if permissible, increasing m or reducing h_0 would further broaden the BGs.

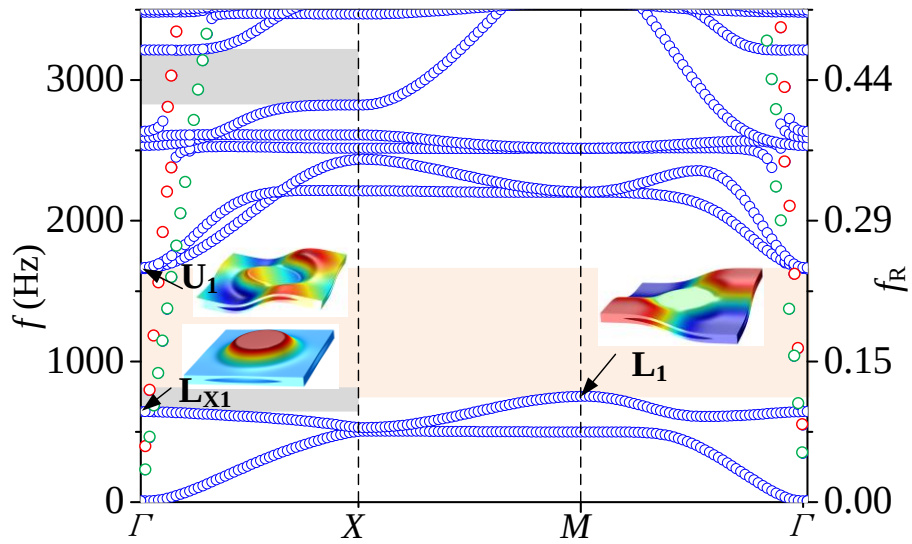

Fig. 10 Band structures of periodic ABH plates with a connecting cylinder with radius r=20 mm.

The effect of the normalized radius r/a on BGs is investigated and shown in Fig. 11. Here, only the cylinder radius is changed while all other geometrical parameters, a, h_0, m and l_{ABH}, are kept the same as before. Keep in mind that the whole length of

ABH taper l_{ABH} -r also changes accordingly. Fig. 11 shows that increasing r/a up to 0.2 would broaden the BG, alongside a simultaneous reduction in the lower frequency bound and an increase in the upper one, as a direct benefit of the enhanced Bragg scattering effect. However, a further increase in r/a would shrink the bandwidth oppositely, since the whole length of ABH taper l_{ABH} -r is excessively reduced so that the necessary ABH-induced local resonances are compromised. Therefore, there exists an optimal size for the connecting cylinder to balance the dual effect of local resonance and Bragg scattering to achieve the broadest BGs.

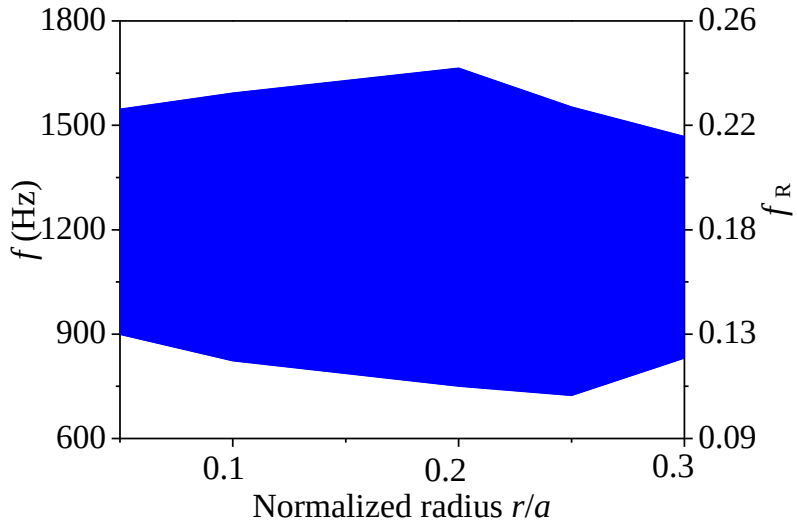

Fig. 11 Effect of normalized r/a on BGs.

Analyses are also conducted on a finite freely-supported plate containing 6×4 cells with connecting cylinders to demonstrate its vibration insulation ability. Using the same pair of excitation and receiver points as before, Fig. 12 shows the displacement transmissibility curve. A very broad band with drastic vibration attenuation appears, which is consistent with the BG (marked by pink area) obtained in infinite periodic plate. This high level of attenuation is obtained by using only a small number of cells in the plate. The inset at 1180 Hz which is within the attenuation band also confirms that the vibration energy is highly concentrated in the half part of the first cell due to the reflections from the supporting cylinder. The enhanced Bragg scattering entails effective wave attenuation when reaching roughly

the third row of the ABH cells, demonstrating the extremely high ability of the proposed structure in vibration insulation. As a comparison, the vibration field at 1180 Hz which is outside the attenuation band shows no obvious energy attenuation trend throughout the plate.

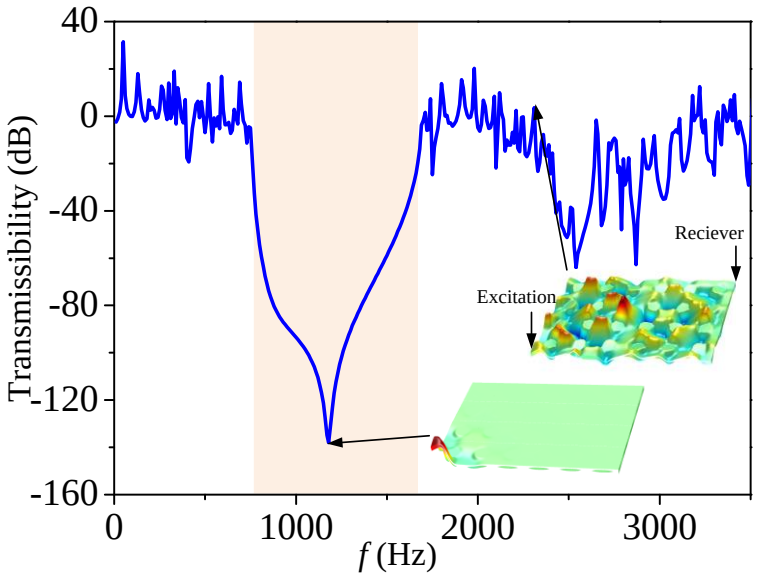

Fig. 12 Displacement transmissibility of a freely-supported finite plate with 6×4 ABH cells with a connecting cylinder inside. Also displayed are the displacement fields at 1180 Hz and 2310 Hz, in and out of the attenuation bands, respectively.

5. Experimental validations

To verify the above revealed phenomena, experiments were carried out on a 3D printed plate containing 6×4 ABH cells with a connecting cylinder. The plate is made of aluminum with a mass density of 2550 kg/m3, Yong's modulus of 70 GPa, Poisson's ratio of 0.3 and a damping loss factor of 0.001. The structural dimensions are given by h=7.2 mm, h_0=0.6mm, m=3, l_{ABH} =50 mm, r=15mm, and a=80 mm. The experimental system is shown in Fig. 13. The plate was suspended by two thin strings to mimic free boundaries. Through an electromagnetic shaker (MB Dynamics MODAL50), a force excitation driven by a periodic chirp signal from 0 to 5 kHz was applied at the left bottom corner of the plate. The excitation force was measured by a force transducer (PCB PIEZOTRONICS 208C02). A Polytec 400 laser vibrometer was used to measure the vibration velocity field by scanning 83×51 equally

distributed points. Both the excitation force and vibration field signals were fed back to a PC with Polytec 400 laser vibrometer system for FFT post-processing. The sampling frequency and sampling time were set at 12.8 kHz and 320 ms, respectively.

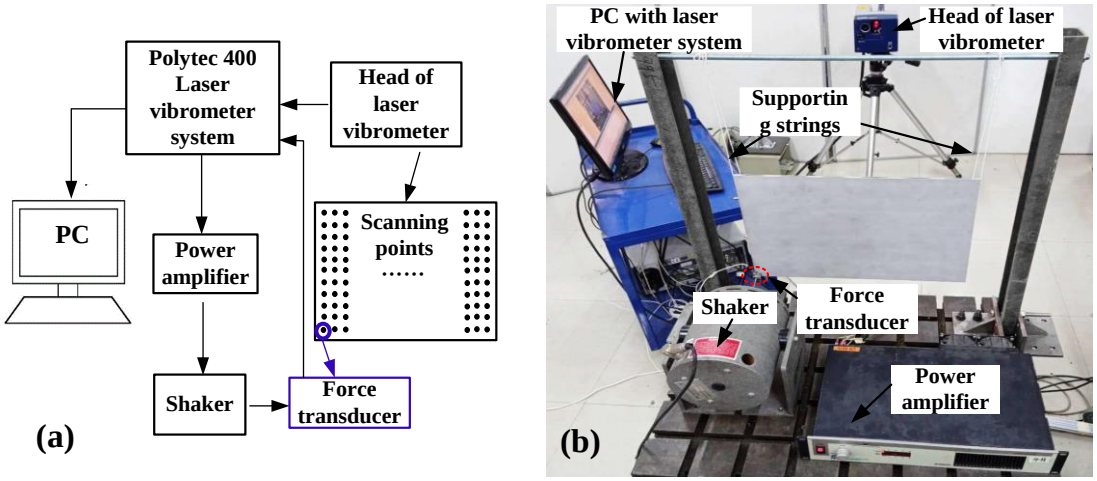

Fig. 13 Experimental system: (a) schematic diagram; (b) Experimental setup

Using the same pair of excitation and receiver points as the one used in the previous simulations, the experimentally measured displacement transmissibility is shown and compared with numerical results in Fig. 14. The experimental results agree well with FEM analyses in terms of both amplitude and resonant frequencies below 3700 Hz. The difference at higher frequencies may be caused by local dimensional errors from the machining and the torsional modes ignored in the simulation, both of which emerge more obviously at higher frequencies. Particularly, a broad attenuation band is observed with a significant transmissibility attenuation , roughly ranging from 2070 Hz to 3590 Hz, showing again a high consistency between experiment and numerical results. It is understandable that the extremely low transmissibility (close to -120 dB) that was numerically predicted could never be reached experimentally, due to the extremely weak vibration level within attenuation band and the inevitable existence of the torsional waves, existing in experiments but ignored in simulations. To better visualize the energy insulation effects, the displacement distributions over the plate at a few representative frequencies inside and outside the attenuation band (as marked by F_1, F_2, F_3, F_4 in Fig. 14) are also shown in Fig. 15. It can be seen that at

the attenuation valley f=2831 Hz (marked by F_1), the vibration reduction is confined to the vicinity of the excitation region with virtually no propagation to the rest of the plate. Even for the local peak frequency at f=3221 Hz (marked by F_2) inside the attenuation band, the vibration reduction from the excitation to receiver points is also considerable as shown in Fig. 15 (b). As to the other two frequencies 1562 Hz and 4284 Hz, both outside the attenuation band, vibration is spread over the entire plate as shown in Fig. 15 (c) and (d). Therefore, the predicted high vibration attenuation ability of the proposed structure is experimentally confirmed.

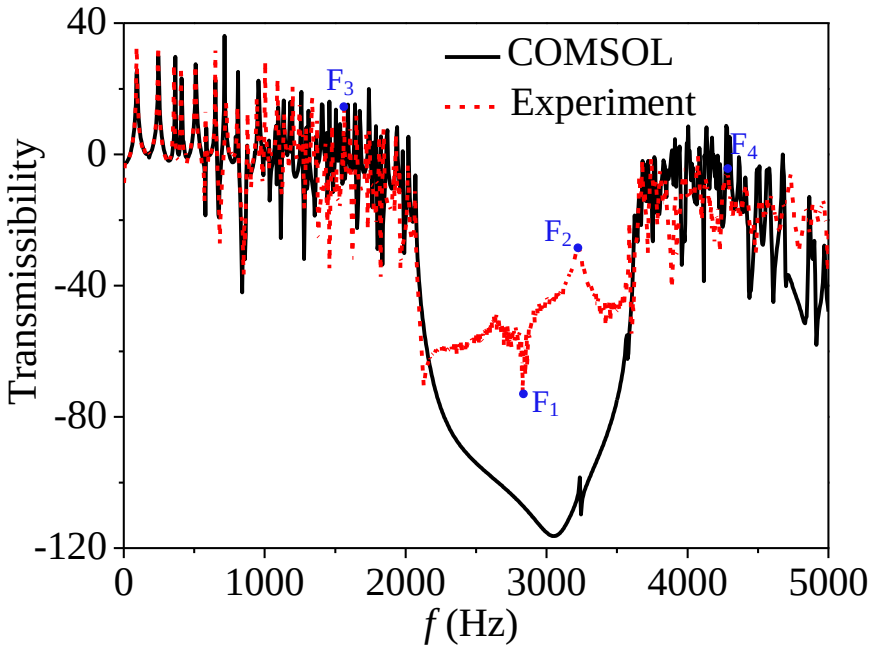

Fig. 14 Displacement transmissibility comparison between experimental (red dashed line) and numerical results (dark solid line).

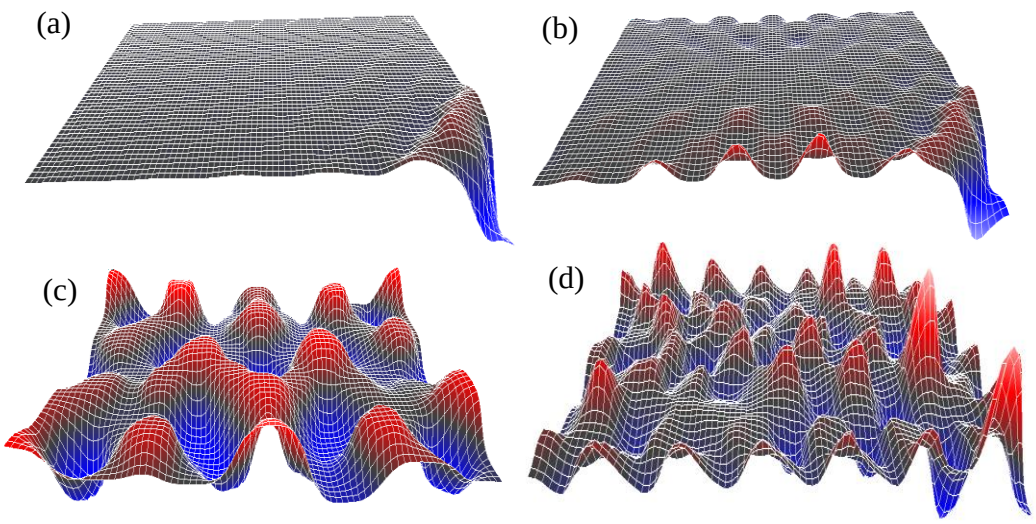

Fig. 15 Experimentally measured displacement distributions at selected frequencies as marked in Fig. 14 inside and outside the transmissibility attenuation band: (a) f=2831 Hz as marked by F_1; (b) f=3221 Hz as marked by F_2; (c) f=1562 Hz as marked by F_3; (d) f= 4284 Hz as marked by F_4.

6. Conclusions

By capitalizing on the ABH-specific wave propagation properties in a 2D ABH plate, a new type of compound double-layer periodic plate is proposed in this paper. Finite element analyses show the existence of complete sub-wavelength BGs in a lattice with periodically arranged compound double-layer ABH unit cells, which are absent in the corresponding single-layer configuration. Numerical analyses on band structures and eigenmodes at the edge points reveal that the formation of these BGs results from the combined effects of local resonances and Bragg scattering, which are fully played out by the proposed design through maximizing the benefits of ABH features.

Analyses show that the effective generation of the BGs is achieved through a dual process: a proper channeling of the wave propagation path and an impaired coupling between the ABH-induced local resonances and the global structural vibration of the unit cells. The former is achieved through a proper tailoring of the

structural configuration and the latter by the specific dynamics of the double-layer ABH design.

As possible means to improve the BG performance, reducing truncation thickness or increasing the taper power index of the ABH thickness profile allows for possible but limited tuning of the BGs properties in terms of lowering the BG frequency and broadening its bandwidth. As a more effective method, adding a small connecting cylinder at the center of the ABH indentation turns out to be a better way to further increase the resultant BGs through enhancing Bragg scattering effect. In all cases, implementing the proposed design principle in finite plates embedded with only a small number of cells can enable remarkable vibration attenuation and energy insulation across the plate. Experiments conducted on a plate of finite size confirm and validate the numerically predicted phenomena and the efficacy of the proposed plate in terms of vibration insulation. Therefore, the proposed plates with a small number of ABH cells can be used as basic building block to conceive effective vibration systems, especially in a sub-wavelength frequency range with structures of reasonable dimension.

Acknowledgements

This work was supported by the National Science Foundation of China (No. 11902260, No.11532006, No. 11974287), Fundamental Research Funds for the Central Universities (No. 3102019HHZY03001), and Research Grant Council of the Hong Kong SAR (PolyU 152017/17E) .

References

[1] M.A. Mironov, Propagation of a flexural wave in a plate whose thickness decreases smoothly to zero in a finite interval, *Soviet Physics: Acoustics* 34 (3) (1988) 318-319.

[2] V. Krylov, Overview of localized flexural waves in wedges of power-law profile and comments on their relationship with the acoustic black hole effect, *Journal of Sound and Vibration* 468 (2020)115100.

[3] V.V. Krylov, and F. J. B. S. Tilman, Acoustic ‘black holes’ for flexural waves as

effective vibration dampers, *Journal of Sound and Vibration* 274 (2004) 605-619.

[4] D.J. O'Boy, V.V. Krylov, Damping of flexural vibrations in circular plates with tapered central holes, *Journal of Sound and Vibration*330 (2011) 2220-2236.

[5] V.B. Georgiev, J. Cuenca, F. Gautier, L. Simon, and V. V. Krylov, Damping of structural vibrations in beams and elliptical plates using the acoustic black hole effect, *Journal of Sound and Vibration* 330 (2011) 2497-2508.

[6] V.V. Krylov, and R.E.T.B. Winward, Experimental investigation of the acoustic black hole effect for flexural waves in tapered plates, *Journal of Sound and Vibration* 300(1-2) (2007) 43-49.

[7] S.C. Conlon, and J.B. Fahnline, Numerical analysis of the vibroacoustic properties of plates with embedded grids of acoustic black holes, *Journal of the Acoustical Society of America* 137(1) (2015) 447-457.

[8] H.L. Ji, X.D. Wang, J.H. Qiu, L. Cheng, Y.P. Wu, and C. Zhang, Noise reduction inside a cavity coupled to a flexible plate with embedded 2-D acoustic black holes, *Journal of Sound and Vibration* 455 (2019) 324-338.

[9] L. Ma, and L. Cheng, Sound radiation and transonic boundaries of a plate with acoustic black hole, *Journal of the Acoustical Society of America* 145 (2019) 164-172.

[10] X.D. Wang, H.L. Ji, J.H. Qiu, and L. Cheng, Wavenumber domain analyses of vibro-acoustic decoupling and noise attenuation in a plate-cavity system enclosed by an acoustic black hole plate, *Journal of the Acoustical Society of America* 146(1) (2019) 72-84.

[11] L.X. Zhao, S.C. Conlon, and F. Semperlotti, Broadband energy harvesting using acoustic black hole structural tailoring, *Smart Materials and Structures* 23 (2014) 065021.

[12] L.X. Zhao, S.C. Conlon, and F. Semperlotti, An experimental study of vibration based energy harvesting in dynamically tailored structures with embedded acoustic black holes, *Smart Materials and Structures* 24 (2015) 065039.

[13] H. Ji, Y. Liang, J. Qiu, L. Cheng, and Y. Wu, Enhancement of vibration based energy harvesting using compound acoustic black holes, *Mechanical Systems and Signal Processing* 132 (2019) 441-456.

[14] V. Denis, F. Gautier, A. Pelat, and J. Poittevin. Measurement and modelling of the reflection coefficient of an acoustic black hole termination, *Journal of Sound*

and Vibration 349 (2015) 67-79.

[15] H. Ji, J. Luo, J. Qiu, and L. Cheng, Investigations on flexural wave propagation and attenuation in a modified one-dimensional acoustic black hole using a laser excitation technique, *Mechanical Systems and Signal Processing* 104 (2018) 19-35.

[16] T. Zhou, and L. Cheng. A resonant beam damper tailored with acoustic black hole features for broad-band vibration reduction, *Journal of Sound and Vibration* 430 (2018) 174-184.

[17] J. Deng, L. Zheng, P. Zeng, Y. Zuo, and O. Guasch. Passive constrained viscoelastic layers to improve the efficiency of truncated acoustic black holes in beams, *Mechanical Systems and Signal Processing* 118 (2019) 461-476.

[18] Y. Wang, J. Du, and L. Cheng, Power flow and structural intensity analyses of Acoustic Black Hole beams, *Mechanical Systems and Signal Processing* 131 (2019) 538-553.

[19] S. Park, M. Kim, and W. Jeon, Experimental validation of vibration damping using an Archimedean spiral acoustic black hole, *Journal of Sound and Vibration* 459 (2019) 114838,

[20] H. Li, C. Touze, A. Pelat, F. Gautier, and X. Kong, A vibro-impact acoustic black hole for passive damping of flexural beam vibrations, *Journal of Sound and Vibration* 450 (2019) 28-46.

[21] L.L. Tang, and L. Cheng, Enhanced Acoustic Black Hole effect in beams with a modified thickness profile and extended platform, *Journal of Sound and Vibration* 391 (2017) 116-126.

[22] L.L. Tang, and L. Cheng, Broadband local resonant bandgaps in periodic structures with embedded acoustic black holes, *Journal of Applied Physics* 121 (2017) 194901.

[23] L.L. Tang, and L. Cheng, Ultrawide band gaps in phononic beams with double-leaf acoustic black hole indentations, *The Journal of the Acoustical Society of America* 142 (2017) 2802-2807.

[24] N. Gao, Z.Wei, H. Hou, and A.O. Krushynska, Design and experimental investigation of v-folded beams with acoustic black hole indentations, *The Journal of the Acoustical Society of America* 145(2019) EL79-EL83.

[25] Y. Zhang, K. Chen, Y. Cheng, and Z. Wei, Lightweight-high-stiffness vibration insulator with ultra-broad band using graded double-leaf acoustic black holes,

Applied Physics Express 13 (2020) 017007.

[26] N. Gao, Z. Wei, R. Zhang, and H. Hou, Low-frequency elastic wave attenuation in a composite acoustic black hole beam, *Applied Acoustics* 154 (2019) 68-76.

[27] H. Zhu, and F. Semperlotti, Phononic thin plates with embedded acoustic black holes, *Physical Review B* 91(10) (2015) 104304.

[28] H. Zhu, and F. Semperlotti, Two-dimensional structure-embedded acoustic lenses based on periodic acoustic black holes, *Journal of Applied Physics* 122 (2017) 065104.

[29] S. S. Ganti, T.-W. Liu, and F. Semperlotti, Topological edge states in phononic plates with embedded acoustic black holes, *Journal of Sound and Vibration* 466 (2020)115060.

[30] L.L. Tang, and L. Cheng, Periodic plates with tunneled Acoustic-Black-Holes for directional band gap generation, *Mechanical Systems and Signal Processing* 135 (2019) 106257.

[31] L.L. Tang, and L. Cheng, Imparied sound radiation in plates with periodic tunneled Acoustic Black Holes, *Mechanical Systems and Signal Processing* 135 (2020) 106410.

[32] W. Huang, H. Ji, J. Qiu, and L. Cheng, Analysis of ray trajectories of flexural waves propagating over generalized acoustic black hole indentations, *Journal of Sound and Vibration* 417 (2018) 21-226.

[33] P.A. Feurtado, and S.C. Conlon, A normalized wave number variation parameter for acoustic black hole design, *The Journal of the Acoustical Society of America* 136(2014) EL148-EL152.